Evaluation and Integration of the Thin Wire Kernel

Donald R. Wilton, *Fellow, IEEE,* and Nathan J. Champagne, *Senior Member, IEEE*

***Abstract*—New approaches for numerically computing the thin wire kernel and wire potential integrals are presented. The singular behavior of the kernel integral is removed by transforming the integration variable to produce a smooth integrand. Subsequent integration of the kernel to obtain potential integrals uses quadrature schemes catering to its behavior. This technique allows standard algorithms for numerical quadrature to be used with updated integration weights that account for the transformed behavior, obviating the need for singularity subtraction techniques. The result is a procedure for evaluating the potential integrals that is independent of the basis functions.**

***Index Terms*—Exact kernel, numerical integration, singularity analysis, wire.**

I. Introduction

TRADITIONALLY, the singularity present in the method of moments (MoM) analysis for wires has been evaluated analytically using singularity extraction techniques [1]–[3]. In the 1990s, an approach that avoids singularity extraction by exactly representing the wire kernel as an infinite series was proposed [4]–[6]. In all these approaches, the basis function must be considered in the analysis. Thus, a new analysis is required for each different basis function, making it difficult, for example, to treat hierarchical bases.

A technique for numerically evaluating an exact expression of the wire kernel was recently proposed [7], [8]. The approach is described in more detail in this paper. Additionally, a procedure using this new kernel expression for evaluating the potentials when they are nearly singular is discussed. This new scheme involves using variable transforms to create a smooth integrand that may be evaluated numerically. Part of this process involves using the quadrature scheme of [9]. Hence, this new approach eliminates the need for singularity extraction, paving the way for use of higher order basis functions on wires in a tractable algorithm.

II. Method of Moments Analysis

The currents on a wire structure are determined using the electric field integral equation (EFIE), given by

$$[\mathbf{E}^i(\mathbf{r}) + \mathbf{E}^s(\mathbf{r})]_{\tan} = 0, \quad \mathbf{r} \in S \tag{1}$$

where S denotes the wire surface. The excitation $\mathbf{E}^i(\mathbf{r})$ may be either an incident electric field or a voltage source. The scattered electric field $\mathbf{E}^s(\mathbf{r})$ is expressed in terms of the magnetic vector and the electric scalar potentials as

$$\mathbf{E}^s(\mathbf{r}) = -j\omega\mathbf{A}(\mathbf{r}) - \nabla\Phi(\mathbf{r}). \tag{2}$$

The potentials are defined as

$$\mathbf{A}(\mathbf{r}) = \frac{\mu}{4\pi}\int_S \frac{\mathbf{I}(\mathbf{r}')}{2\pi a(\mathbf{r}')}\frac{e^{-jkR}}{R}dS' \tag{3}$$

and

$$\Phi(\mathbf{r}) = -\frac{1}{j4\pi\omega\varepsilon}\int_S \nabla'_S \cdot \left(\frac{\mathbf{I}(\mathbf{r}')}{2\pi a(\mathbf{r}')}\right)\frac{e^{-jkR}}{R}dS' \tag{4}$$

where $R = |\mathbf{r} - \mathbf{r}'|$ is the distance between the observation and source points, $k = \omega\sqrt{\mu\varepsilon}$ is the wavenumber of the medium, the vector $\mathbf{I}(\mathbf{r})$ represents both the direction and complex amplitude of the total current, and $a(\mathbf{r})$ is the (piecewise constant) wire radius at $\mathbf{r}$. The quantities μ and ε are the permeability and permittivity of the medium, respectively. The unknown current on the wire structure is approximated as

$$\mathbf{I}(\mathbf{r}) \approx \sum_{n=1}^{N} I_n \mathbf{\Lambda}_n(\mathbf{r}), \quad \mathbf{r} \in S \tag{5}$$

where I_n is the n th unknown current coefficient and $\mathbf{\Lambda}_n(\mathbf{r})$ is a vector basis function used to represent the current on the wire. Note that the wire is considered to be thin so that $\mathbf{\Lambda}_n(\mathbf{r})$ has no azimuthal component or variation. Now the potentials may be written in terms of sums of partial potentials arising from the bases $\mathbf{\Lambda}_n(\mathbf{r})$ as

$$\mathbf{A}(\mathbf{r}) = \frac{\mu}{4\pi}\sum_{n=1}^{N} I_n \int_S \frac{\mathbf{\Lambda}_n(\mathbf{r}')}{2\pi a(\mathbf{r}')}\frac{e^{-jkR}}{R}dS' \tag{6}$$

and

$$\Phi(\mathbf{r}) = -\frac{1}{j4\pi\omega\varepsilon}\sum_{n=1}^{N} I_n \int_S \frac{\nabla'_S \cdot \mathbf{\Lambda}_n(\mathbf{r}')}{2\pi a(\mathbf{r}')}\frac{e^{-jkR}}{R}dS' \tag{7}$$

where the wire radius is constant on each segment and has been removed from the divergence in (7) since, as demonstrated in [10], no condition on the charge at stepped-radius connections between wires is necessary.

Equations (6) and (7) may be written in terms of the wire segment geometry by letting $dS' = a(\mathbf{r}')d\phi' d\ell'$, where $d\ell'$ is a differential arc length along the wire axis ℓ and $d\phi'$ is an angle differential measured about the wire circumference. The vector and scalar potentials thus become

$$\mathbf{A}(\mathbf{r}) = \mu\sum_{n=1}^{N} I_n \int_\ell \mathbf{\Lambda}_n(\mathbf{r}')K(\mathbf{r},\mathbf{r}')d\ell' \tag{8}$$

Manuscript received August 8, 2005; revised December 3, 2005.

D. R. Wilton is with the Department of Electrical and Computer Engineering, University of Houston, Houston, TX 77204-4005 USA (e-mail: wilton@uh.edu).

N. J. Champagne is with the Electrical Engineering Program, Louisiana Tech University, Ruston, LA 71272 USA (e-mail: champagn@latech.edu).

Digital Object Identifier 10.1109/TAP.2005.872569

and

$$\Phi(\mathbf{r}) = \frac{-1}{j\omega\varepsilon} \sum_{n=1}^{N} I_n \int_{\ell} \nabla'_S \cdot \mathbf{\Lambda}_n(\mathbf{r}') K(\mathbf{r}, \mathbf{r}') d\ell' \tag{9}$$

where

$$K(\mathbf{r}, \mathbf{r}') = \frac{1}{2\pi} \int_{-\pi}^{\pi} \frac{e^{-jkR}}{4\pi R} d\phi' \tag{10}$$

is the wire kernel. In (8)–(10), $\mathbf{r}'$ is reinterpreted as a vector to a point on the wire axis; R is no longer $|\mathbf{r} - \mathbf{r}'|$, but is the distance from $\mathbf{r}$ to a point with angle parameter ϕ' on the wire's cross section centered at $\mathbf{r}'$. Since, under thin-wire assumptions, the surface current (and basis) does not vary about the wire's cross section, the basis $\mathbf{\Lambda}_n(\mathbf{r}')$ may be associated with $\mathbf{r}'$.

The evaluation of (8) and (9) is usually reduced to its partial contributions from each linear wire segment (element) ΔL comprising the wire model. Since the vector bases for current have constant direction on each linear segment, both required potential integrals reduce to scalar integrals of the form

$$\int_{\Delta L} B(\mathbf{r}') K(\mathbf{r}, \mathbf{r}') d\ell' \tag{11}$$

where $B(\mathbf{r})$ is a scalar current or charge basis. The evaluation of (11) requires two steps: first, the kernel $K(\mathbf{r}, \mathbf{r}')$ (10) is evaluated, and then the integral (11) is performed. These steps are discussed in the next two sections.

III. Evaluation of the Wire Kernel

Because of the rotational symmetry of both sources and their potentials about a linear tubular section, we can consider, without loss of generality, an observation point in cylindrical coordinates at $(\rho, 0, z)$ and sources on a cylindrical tube of constant radius a centered along the z axis and with a circumferentially invariant, z-directed current as shown in Fig. 1. The wire kernel is defined as

$$\begin{aligned} K(\mathbf{r}, \mathbf{r}') = K(\rho, z - z') &= \frac{1}{2\pi} \int_{-\pi}^{\pi} \frac{e^{-jkR}}{4\pi R} d\phi' \\ &= \frac{1}{4\pi^2} \int_{0}^{\pi} \frac{e^{-jkR}}{R} d\phi' \end{aligned} \tag{12}$$

where $R = \sqrt{(z - z')^2 + \rho^2 + a^2 + 2\rho a \cos\phi'}$. The kernel represents the potential of a scalar ring source of radius a located at $z = z'$. With the substitution $\alpha = (\pi - \phi')/2$ and application of standard trigonometric identities, R may be written as

$$\begin{aligned} R &= \sqrt{(z - z')^2 + (\rho + a)^2 - 4\rho a \sin^2\alpha} \\ &= R_{\max} \sqrt{1 - \beta^2 \sin^2\alpha} \end{aligned} \tag{13}$$

where $R_{\max} = \sqrt{(z - z')^2 + (\rho + a)^2}$ is the distance to the farthest point on the tube cross section at z' and $\beta^2 = 4\rho a / R_{\max}^2$. A geometrical visualization of quantities forming the ratio $\beta = 2\rho_G / R_{\max}$, where $\rho_G = \sqrt{\rho a}$ is the geometrical mean radius, is illustrated in Fig. 2. These expressions may be substituted into (12), allowing the kernel to be rewritten as

$$\begin{aligned} K(\rho, z - z') = &\frac{1}{2\pi^2 R_{\max}} \\ &\times \int_{0}^{\pi/2} \frac{e^{-jkR_{\max}\sqrt{1-\beta^2\sin^2\alpha}}}{\sqrt{1 - \beta^2 \sin^2\alpha}} d\alpha. \end{aligned} \tag{14}$$

To cancel possible singularities present in (14), the following transformation is used:

$$u = F(\alpha, \beta) = \int_{0}^{\alpha} \frac{d\alpha}{\sqrt{1 - \beta^2 \sin^2\alpha}} \tag{15}$$

where $F(\alpha, \beta)$ is the incomplete elliptic integral of the first kind; the corresponding inverse function is the Jacobi amplitude function $\alpha = \mathrm{am}(u \,|\, \beta)$. Noting that

$$du = \frac{\partial}{\partial\alpha} F(\alpha, \beta) d\alpha = \frac{d\alpha}{\sqrt{1 - \beta^2 \sin^2\alpha}} \tag{16}$$

the wire kernel is thus transformed to

$$\begin{aligned} K(\rho, z - z') &= \frac{1}{2\pi^2 R_{\max}} \\ &\quad \times \int_{0}^{K(\beta)} e^{-jkR_{\max}\sqrt{1-\beta^2\mathrm{sn}^2 u}} du \\ &= \frac{1}{2\pi^2 R_{\max}} \int_{0}^{K(\beta)} e^{-jkR_{\max}\mathrm{dn}u} du \end{aligned} \tag{17}$$

where $F(\pi/2, \beta) = K(\beta)$ is the complete elliptic integral of the first kind, and $\mathrm{sn}u = \sin\alpha$ and $\mathrm{dn}u = \sqrt{1 - \beta^2 \mathrm{sn}^2 u}$ are Jacobi elliptic functions.

One observes that the transformation (15) cancels potential singularities in (14). Further, when the thin wire assumption

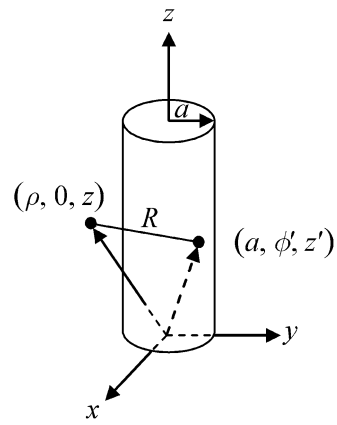

Fig. 1. Geometry used for wire kernel evaluation.

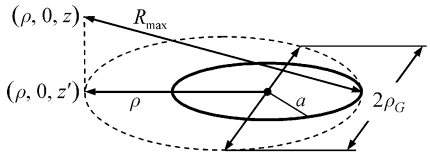

Fig. 2. Geometrical interpretation of $\beta = 2\rho_G / R_{\max}$.

$ka \ll 1$ holds, the resulting integrand of the transformed integral (17) is extremely smooth since the phase variation of $kR = kR_{\max}\mathrm{dn}u$ is at most $2ka$, independent of observation point. Hence, (17) is useful not only in computing singular (self) terms, but also in computing near singular terms that arise from closely spaced wires or between a wire and its image in a nearby ground plane.

An excellent approximation of the exact kernel for thin wires is readily obtained from (17) by expanding the integrand in the following two term series

$$e^{-jkR_{\max}\mathrm{dn}u} = e^{-jkR_{\max}}e^{-jkR_{\max}(\mathrm{dn}u-1)} \approx e^{-jkR_{\max}}[1-jkR_{\max}(\mathrm{dn}u-1)]. \quad (18)$$

The resulting integrand may be integrated term by term, yielding

$$K(\rho, z-z') \approx \frac{e^{-jkR_{\max}}}{2\pi^2 R_{\max}} K(\beta)\left[1-jkR_{\max}\left(\frac{\pi/2}{2(\beta)}-1\right)\right] \quad (19)$$

where the complete elliptic integral factor incorporates the logarithmic behavior of the kernel for observation points near the ring source, while the spherical wave factor highlights its point-source-like behavior far from the source. Use of approximate forms is quite unnecessary in practice, however, as the integral (17) may be efficiently evaluated numerically to essentially arbitrary accuracy using Gauss-Legendre rules of relatively low order. This is done by approximating (17) as

$$K(\rho, z-z') \approx \frac{K(\beta)}{2\pi^2 R_{\max}} \sum_{j=1}^{J} w_j^{\mathrm{GL}} e^{-jkR_{\max}\mathrm{dn}\left[\xi^{\mathrm{GL}(j)}K(\beta)\right]} \quad (20)$$

where w_j^{GL} and $\xi^{\mathrm{GL}(j)}$ are weights and sample points, respectively, for a J-point Gauss-Legendre quadrature on the unit interval (0,1). The complete elliptic integral and Jacobi elliptic function are readily computed via algorithms given in [11] and [12], respectively.

Examination of series representations for complete elliptic integrals reveals that as $z \to z', K(\rho, z-z')$ behaves as $P(z-z') + Q(z-z')\ln|z-z'|$ where $P(x)$ and $Q(x)$ are analytic functions of x. Hence the z' integration along the tube needed for an integral equation solution may be carried out using the quadrature rules of [9]. (This approach can also be extended to bodies of revolution since, in addition to the phase factor e^{-jkR}, the integrand (17) contains only the additional circumferential phase factor $e^{jn\phi'}$. This simply places a greater burden on the circumferential integration.)

IV. Integration of the Wire Kernel

Next, the evaluation of the potential integral (11) is considered. As in the previous section, it is assumed that the wire segment is placed such that the wire axis is parallel to the z axis as shown in Fig. 3. The integral over the segment is parameterized in terms of z'; basis functions are generally expresssed in terms of local normalized coordinates (ξ_1, ξ_2) as defined later. When

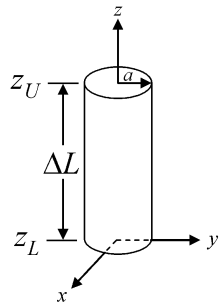

Fig. 3. Geometry of a wire segment.

the observation point is far from the source, the required integral is easily evaluated by numerical quadrature as

$$\begin{aligned}\int_{z_L}^{z_U} B(\xi_1,\xi_2)K(z,z')dz' &= \Delta L\int_0^1 B(\xi_1,\xi_2)K(z, z_L\xi_1 + z_U\xi_2)d\xi_1 \\ &\approx \Delta L\sum_{k=1}^{K} w_k B\left(\xi_1^{(k)},\xi_2^{(k)}\right)K\left(z, z^{(k)}\right) \end{aligned} \quad (21)$$

where $\Delta L = z_U - z_L$ is the segment length and $B(\xi_1, \xi_2)$ is a vector or scalar basis function expressed in normalized coordinates on the wire segment

$$(\xi_1, \xi_2) = \left(\frac{z_U - z'}{\Delta L}, \frac{z' - z_L}{\Delta L}\right) \quad (22)$$

with $\xi_2 + \xi_1 = 1$, and $K(z, z^{(k)})$ is the wire kernel sampled at source point $z^{(k)}$ at a fixed observation point z. The weights of an appropriate quadrature scheme such as Gauss-Legendre on the normalized interval (0,1) are w_k, and the corresponding sample points are $(\xi_1^{(k)}, \xi_2^{(k)} = 1 - \xi_1^{(k)})$. The goal in the following is to develop an efficient quadrature rule for *singular* and *near-singular* integrands that is *formally identical* to (21) so that no changes need be made in defining or using the bases and kernel; this greatly simplifies the structure and the writing of object-oriented programs that incorporate these integrals. The only caveat is that the new quadrature rule necessarily depends on the observation point $(\rho, 0, z)$.

When the observation point is near or on the wire segment, the location of its projection onto the wire segment axis needs to be determined. In normalized segment coordinates, the projection coordinates are written as

$$\left(\xi_1^0, \xi_2^0\right) = \left(\frac{z_U - z}{\Delta L}, \frac{z - z_L}{\Delta L}\right) \quad (23)$$

and are illustrated in Fig. 4. The integral in (21) is then split, in general, into four regions according to the different kernel behaviors on the wire subsegments as

$$\begin{aligned}&\int_{z_L}^{z_U} B(\xi_1,\xi_2)K(z,z')dz' \\ &= \left[\int_{z_L}^{z-\Delta z_1} + \int_{z-\Delta z_1}^{z} + \int_{z}^{z+\Delta z_2} + \int_{z+\Delta z_2}^{z_U}\right] B(\xi_1,\xi_2)K(z,z')dz' \\ &= I_1 + I_2 + I_3 + I_4 \end{aligned} \quad (24)$$

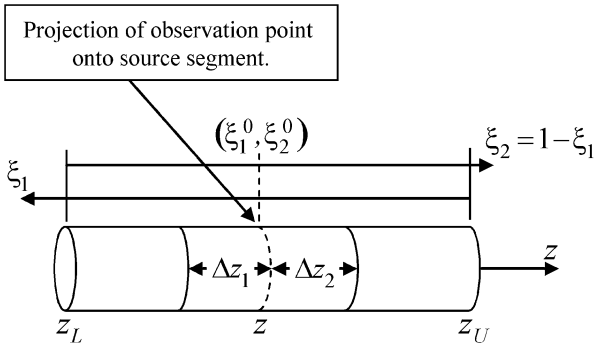

Fig. 4. Splitting of a wire segment into four subsegments.

where Δz_1 and Δz_2 are depicted in Fig. 4. The kernel is dominated by a logarithmic behavior in a neighborhood (Δz_1 and Δz_2) about the projection point. This must be accounted for in the integrals I_2 and I_3. Outside this neighborhood, however, the wire kernel has essentially a $1/R$ behavior that is treated in I_1 and I_4.

In practice, we have found the choice $\Delta z_1, \Delta z_2 \leq \Delta z = 5a$ to be convenient. Hence, as the radius decreases, so does the subsegment length Δz, which may be written in normalized coordinates as $\Delta z = \Delta L \Delta \xi$. However, the $1/R$ behavior replacing the logarithmic behavior over the remainder of the segment is accurately determined using I_1 and I_4. Hence, the analysis remains valid even as the radius approaches zero.

The first integral

$$I_1 = \int_{z_L}^{z-\Delta z_1} B(\xi_1, \xi_2) K(z, z') dz' \tag{25}$$

has a kernel dominated by a $1/R$ behavior. Canceling this behavior, hence smoothing the integrand, is achieved by letting

$$dz' = R_{\max} du = \sqrt{(z-z')^2 + (\rho+a)^2}\, du \tag{26}$$

or, upon integrating

$$u = \sinh^{-1} \frac{z'-z}{\rho+a} = \sinh^{-1} \frac{\Delta L(\xi_2 - \xi_2^0)}{\rho+a}. \tag{27}$$

Since $z' = z + (\rho+a)\sinh u$, (25) may now be written as

$$\begin{aligned} I_1 &= \int_{u_{1L}}^{u_{1U}} B(\xi_1, \xi_2) K\left[z, z+(\rho+a)\sinh u\right] R_{\max} du \\ &\approx \Delta L \sum_{k=1}^{K_1} \left[\frac{w_k^{\mathrm{GL}} (u_{1U} - u_{1L}) R_1^{(k)}}{\Delta L} \right] B\left(\xi_1^{(k)}, \xi_2^{(k)}\right) K\left(z, z^{(k)}\right) \end{aligned} \tag{28}$$

where

$$u_{1L} = -\sinh^{-1} \frac{\Delta L \xi_2^0}{\rho+a}$$

$$u_{1U} = -\sinh^{-1} \frac{\Delta L \max\left(\Delta\xi_1, -\xi_1^0\right)}{\rho+a} \tag{29}$$

$$R_1^{(k)} = (\rho+a)\cosh u_1^{(k)} \tag{30}$$

$$u_1^{(k)} = u_{1L}\xi_1^{\mathrm{GL}(k)} + u_{1U}\xi_2^{\mathrm{GL}(k)} \tag{31}$$

$$z^{(k)} = z + (\rho+a)\sinh u^{(k)} \tag{32}$$

$$\xi_2^{(k)} = \xi_2^0 + \frac{\rho+a}{\Delta L}\sinh u_1^{(k)}, \left(\xi_1^{(k)} = 1 - \xi_2^{(k)}\right) \tag{33}$$

and

$$\Delta\xi_1 = \frac{\Delta z_1}{\Delta L} = \min\left(\xi_2^0, \Delta\xi\right). \tag{34}$$

Since the integrand in the variable u is smooth, the weights w_k^{GL} and samples $(\xi_1^{\mathrm{GL}(k)}, \xi_2^{\mathrm{GL}(k)})$ chosen are those of the Gauss-Legendre scheme on the unit interval (0,1). The bracketed quantity in (28) and expression (33) represent the new weights and sample points, respectively, mapped back to the original integration domain. Additionally, the expression for $\Delta\xi_1$ in (34) controls the upper limit of integration in (29). If the projected observation point falls such that $z < z_L + \Delta z$, then (34) limits the upper limit to ξ_2^0. This results in identical upper and lower limits so that $I_1 = 0$. Correspondingly, we also set $K_1 = 0$. When the projected observation point falls past the opposite segment endpoint ($\xi_1^0 < 0$) such that $-\xi_1^0 > \Delta\xi$, then the upper limit of integration in (29) is limited to $-\xi_1^0$, resulting in I_1 being evaluated over the entire segment. The contributions from I_2, I_3, and I_4 are zero in this case.

The fourth integral I_4 is analogous to I_1 and may be similarly evaluated, yielding

$$\begin{aligned} I_4 &= \int_{z+\Delta z_2}^{z_U} B(\xi_1, \xi_2) K(z, z') dz' \\ &= \int_{u_{4L}}^{u_{4U}} B(\xi_1, \xi_2) K(z, z+(\rho+a)\sinh u) R_{\max} du \\ &\approx \Delta L \sum_{k=1}^{K_4} \left[\frac{w_k^{\mathrm{GL}} (u_{4U} - u_{4L}) R_4^{(k)}}{\Delta L} \right] \\ &\quad \times B\left(\xi_1^{(k)}, \xi_2^{(k)}\right) K\left(z, z^{(k)}\right) \end{aligned} \tag{35}$$

where $\xi_1^{(k)}$ and $\xi_2^{(k)}$ are defined as in (33), $z^{(k)}$ is defined as in (32)

$$u_{4L} = \sinh^{-1} \frac{\Delta L \max\left(\Delta\xi_2, -\xi_2^0\right)}{\rho+a}$$

$$u_{4U} = \sinh^{-1} \frac{\Delta L \xi_1^0}{\rho+a} \tag{36}$$

$$R_4^{(k)} = (\rho+a)\cosh u_4^{(k)} \tag{37}$$

$$u_4^{(k)} = u_{4L}\xi_1^{\mathrm{GL}(k)} + u_{4U}\xi_2^{\mathrm{GL}(k)} \tag{38}$$

and

$$\Delta\xi_2 = \frac{\Delta z_2}{\Delta L} = \min\left(\xi_1^0, \Delta\xi\right). \tag{39}$$

Here, as with I_1, the bracketed quantity in (35) represents the weights mapped back to the original integration domain. Also, similar to I_1, (39) controls the integration limits. When $\max(\Delta\xi_2, -\xi_2^0) = -\xi_2^0$ in (36), the lower limit of integration is such that I_4 covers the entire segment. When $\Delta\xi \geq \xi_1^0$, the fourth integral is zero ($I_4 = 0$), and we correspondingly set $K_4 = 0$.

The integral I_2 has a logarithmic singularity that may be handled using the Ma, Rohklin, Wandzura (MRW) quadrature

scheme [9]. With the substitution $z' = z - \xi_2^{\mathrm{MRW}} \Delta L \Delta\xi_1$, the integral becomes

$$\begin{aligned} I_2 &= \int_{z-\Delta z_1}^{z} B(\xi_1,\xi_2) K(z,z')dz' \\ &= \Delta L \Delta\xi_1 \int_0^1 B(\xi_1,\xi_2) K(z,z') d\xi_2^{\mathrm{MRW}} \\ &\approx \Delta L \sum_{k=1}^{K_2} \left[\Delta\xi_1 w_k^{\mathrm{MRW}}\right] B\left(\xi_1^{(k)},\xi_2^{(k)}\right) K\left(z,z^{(k)}\right) \end{aligned} \quad (40)$$

where

$$\begin{aligned} \xi_2^{(k)} &= \xi_2^0 - \xi_2^{\mathrm{MRW}(k)} \Delta\xi_1, \left(\xi_1^{(k)} = 1 - \xi_2^{(k)}\right) \\ z^{(k)} &= z - \xi_2^{\mathrm{MRW}(k)} \Delta L \Delta\xi_1 \end{aligned} \quad (41)$$

and w_k^{MRW} and $\xi_2^{\mathrm{MRW}(k)}$ are the weights and sample points, respectively, of the MRW approach. Similarly, the expression for I_3 is determined using the same approach as I_2, yielding

$$\begin{aligned} I_3 &= \int_{z}^{z+\Delta z_2} B(\xi_1,\xi_2) K(z,z')dz' \\ &= \Delta L \Delta\xi_2 \int_0^1 B(\xi_1,\xi_2) K(z,z') d\xi_2^{\mathrm{MRW}} \\ &\approx \Delta L \sum_{k=1}^{K_3} \left[\Delta\xi_2 w_k^{\mathrm{MRW}}\right] B\left(\xi_1^{(k)},\xi_2^{(k)}\right) K\left(z,z^{(k)}\right) \end{aligned} \quad (42)$$

where

$$\begin{aligned} \xi_2^{(k)} &= \xi_2^0 + \xi_2^{\mathrm{MRW}(k)} \Delta\xi_2, \left(\xi_1^{(k)} = 1 - \xi_2^{(k)}\right) \\ z^{(k)} &= z + \xi_2^{\mathrm{MRW}(k)} \Delta L \Delta\xi_2. \end{aligned} \quad (43)$$

When the projected observation point falls outside of and within Δz of a segment endpoint, then a nearly-singular kernel results that may be difficult to evaluate accurately. For this situation, either $\Delta\xi_1 < 0$ and $\Delta\xi_2 > 0$ or $\Delta\xi_1 > 0$ and $\Delta\xi_2 < 0$ is true as calculated using (34) and (39). The result is that the domain of either I_2 or I_3 extends beyond the segment endpoint to the projected observation point. The remaining integral negates this fictitious contribution from the projected observation point back to the segment endpoint. Thus, the near-singularity is handled by introducing an artificial singularity at the projected observation point in both integrals that permits using the effective MRW scheme for both. Since the integration intervals are necessarily different, the resulting cancellation does not result in a loss of accuracy. Finally, both I_2 and I_3 are zero $(K_2 = K_3 = 0)$ if the projected observation point falls off the segment and does not fall within Δz of a segment endpoint ($\xi_2^0 < -\Delta\xi$ or $\xi_1^0 < -\Delta\xi$).

The list of weights and sample points determined for subintervals I_1, I_2, I_3, and I_4 may be concatenated to produce weights and sample points for a quadrature rule spanning the entire original integration domain as follows:

$$\begin{aligned} w_k &= \frac{w_k^{\mathrm{GL}}(u_{1U} - u_{1L}) R_1^{(k)}}{\Delta L}, & k &= 1,\ldots,K_1 \\ w_{k+K_1} &= \Delta\xi_1 w_k^{\mathrm{MRW}}, & k &= 1,\ldots,K_2 \end{aligned}$$

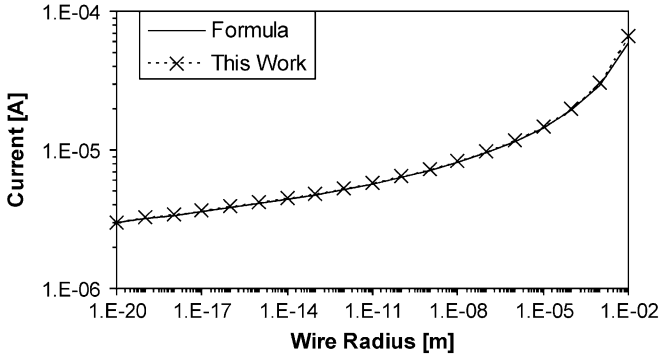

Fig. 5. Imaginary part of wire current at dipole center as wire radius is decreased.

$$\begin{aligned} w_{k+K_1+K_2} &= \Delta\xi_2 w_k^{\mathrm{MRW}}, & k &= 1,\ldots,K_3 \\ w_{k+K_1+K_2+K_3} &= \frac{w_k^{\mathrm{GL}}(u_{4U} - u_{4L}) R_4^{(k)}}{\Delta L}, & k &= 1,\ldots,K_4 \end{aligned} \quad (44)$$

and

$$\begin{aligned} \xi_2^{(k)} &= \xi_2^0 + \frac{\rho + a}{\Delta L} \sinh u_1^{(k)}, & k &= 1,\ldots,K_1 \\ \xi_2^{(k+K_1)} &= \xi_2^0 - \xi_2^{\mathrm{MRW}(k)} \Delta\xi_1, & k &= 1,\ldots,K_2 \\ \xi_2^{(k+K_1+K_2)} &= \xi_2^0 + \xi_2^{\mathrm{MRW}(k)} \Delta\xi_2, & k &= 1,\ldots,K_3 \\ \xi_2^{(k+K_1+K_2+K_3)} &= \xi_2^0 + \frac{\rho + a}{\Delta L} \sinh u_4^{(k)}, & k &= 1,\ldots,K_4 \\ \xi_1^{(k)} &= 1 - \xi_2^{(k)}, & k &= 1,\ldots,K_1 + K_2 \\ & & &\quad + K_3 + K_4. \end{aligned} \quad (45)$$

The new weights and sample points, (44) and (45), which depend on the observation point, may now be used in (21).

V. Results

To demonstrate the robustness of this approach for extremely thin wires, the current on a wire dipole is calculated for a decreasing wire radius. Then, the current on a longer dipole is determined and compared with results from MININEC [13], which uses a method of moments formulation to solve for the currents on a wire. Finally, results from a transmission line are presented to test the formulation's ability to model closely spaced wires. Note that linear basis functions are used in all these cases.

The imaginary part of the current at the center of a 25-cm dipole is plotted versus the wire radius in Fig. 5. The dipole is excited by a unit delta-gap source at 3 MHz. Only two segments were used to model the dipole. The results from this formulation are compared with data generated using an asymptotic expansion for the current [14]. There is good agreement between the two approaches as indicated in the figure. Note that only the imaginary part of the current is presented since the real part is much less than the imaginary part.

A 1-meter dipole with a radius of 1 mm is excited at the center by a unit delta-gap voltage source at 300 MHz. The formulation presented in this paper is compared with MININEC. The dipole is modeled with 20 straight segments. The real and imaginary currents on the dipole are presented in Figs. 6 and 7. The data generated using this formulation show good agreement

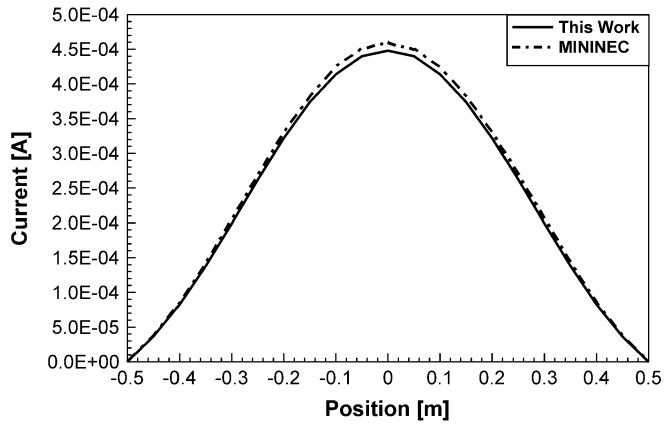

Fig. 6. Real part of current on a 1.0-m dipole.

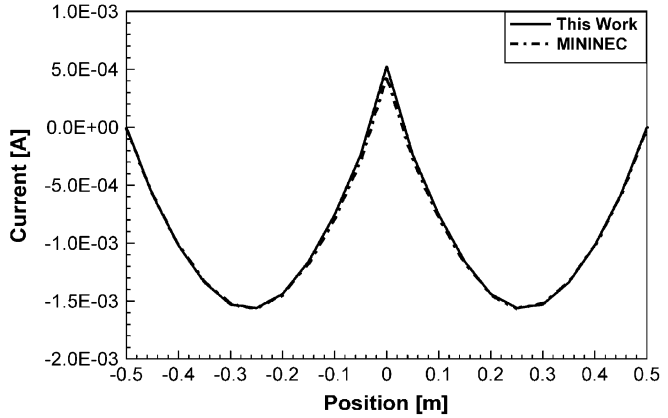

Fig. 7. Imaginary part of current on a 1.0-m dipole.

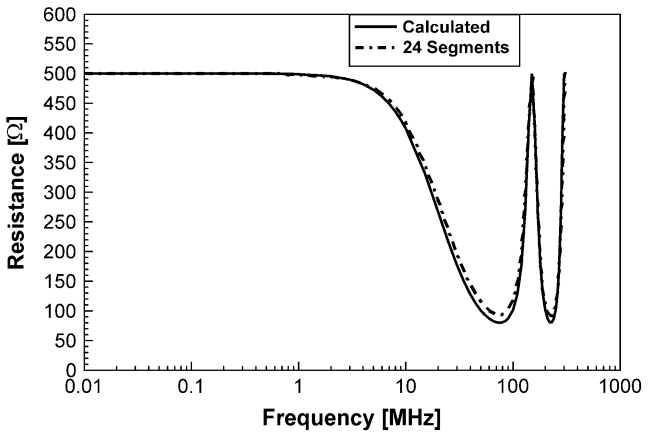

Fig. 8. Input resistance of a transmission line.

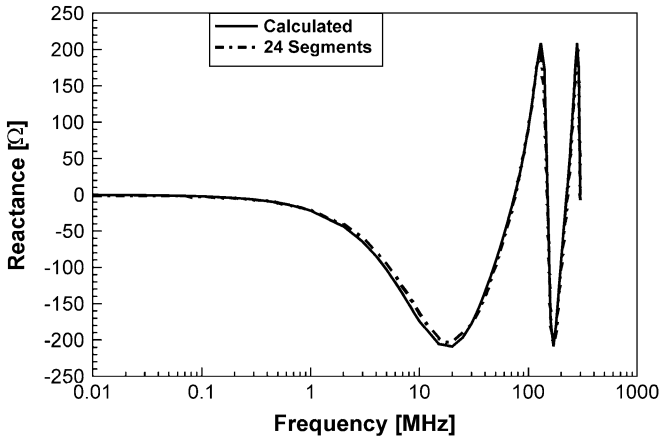

Fig. 9. Input reactance of a transmission line.

with MININEC in the figures. The small differences observed may be due to slight differences in the testing quadrature scheme or in the improved kernel evaluation of the present scheme.

A transmission line is composed of two parallel wires with radii of 1 mm. The length of the line is 1 m. The separation between the wires is 3 mm, leaving a space between the wires of only 1 mm. The parallel wires are connected at each end by two wire segments, each of radius 1 mm. A unit delta-gap voltage source is placed between one pair of segments at one end of the transmission line, and a lumped 500 Ω load is connected between the pair of wires at the other end. A total of 24 segments is used to model the transmission line. The input resistance and reactance of the line are shown in Figs. 8 and 9, respectively. The simulation data are plotted along with data generated using the standard formula for input impedance of the corresponding transmission line section. The numerical data are clearly in excellent agreement with the formula. Note also that as the frequency decreases, both the resistance and reactance data tend toward their respective dc values.

VI. Summary and Conclusion

A procedure for evaluating the potential integrals on wires as the distance between the source and observation points decreases has been presented. The new approach employs a recent technique for numerically evaluating an expression for the exact wire kernel. The formulation is stable for extremely thin and for closely-coupled wires. Since the procedure is not dependent on the form of the basis function, it is readily adapted to algorithms using higher order basis functions. Furthermore, the formulation sets the stage for using higher order wire segments without singularity extraction as well. We expect to report on these developments in the near future.

Acknowledgment

The authors wish to thank Dr. W. A. Johnson of Sandia National Laboratories for his assistance with the asymptotic expansion for the current on a short wire dipole.

References

[1] C. M. Butler, "Evaluation of potential integral at singularity of exact kernel in thin-wire calculations," *IEEE Trans. Antennas Propag.*, vol. 23, no. 2, pp. 293–295, 1975.

[2] C. M. Butler and D. R. Wilton, "Effective methods for solving integral and integro-differential equations," in *Moment Methods in Antennas and Scattering*, R. C. Hansen, Ed. Boston, MA: Artech, 1990, pp. 58–77.

[3] D. H. Werner, J. A. Huffman, and P. L. Werner, "Techniques for evaluating the uniform current vector potential at the isolated singularity of the cylindrical wire kernel," *IEEE Trans. Antennas Propag.*, vol. 42, no. 11, pp. 1549–1553, 1994.

[4] W.-X. Wang, "The exact kernel for cylindrical antenna," *IEEE Trans. Antennas Propag.*, vol. 39, no. 4, pp. 434–435, 1991.

[5] D. H. Werner, "An exact formulation for the vector potential of a cylindrical antenna with uniformly distributed current and arbitrary radius," *IEEE Trans. Antennas Propag.*, vol. 41, no. 8, pp. 1009–1018, 1993.

[6] D. H. Werner, J. A. Huffman, and P. L. Werner, "An exact formulation for the electromagnetic fields of a cylindrical antenna with a triangular current distribution," *Radio Sci.*, vol. 31, no. 4, pp. 701–714, July–Aug. 1996.
[7] M. A. Khayat and D. R. Wilton, "Evaluation of singular and near-singular potentials," presented at the Proc. IEEE AP-S Int. Symp. North American URSI Radio Science Meeting, Columbus, OH, Jun. 22-27, 2003.
[8] M. Khayat and D. R. Wilton, "Revisiting the evaluation of potential integrals," *Proc. Int. Conf. Electromagnetics in Advanced Applications*, pp. 83–86, Sep. 2003.
[9] J. Ma, V. Rokhlin, and S. Wandzura, "Generalized gaussian quadrature rules for systems of arbitrary functions," *Siam J. Numer. Anal.*, vol. 33, pp. 971–996, 1996.
[10] A. W. Glisson and D. R. Wilton, "Numerical procedures for handling stepped-radius wire junctions," Univ. Mississippi, San Diego, CA, Mar. 1979. Final Rep., Contract N66001-77-C-0156, Naval Ocean Systems Center.
[11] M. Abramowitz and I. A. Stegun, *Handbook of Mathematical Functions with Formulas, Graphs, and Mathematical Tables*. New York: Dover, 1965.
[12] W. H. Press, W. T. Vetterling, S. A. Teukolsky, and B. R. Flannery, *Numerical Recipes in Fortran: The Art of Scientific Computing*, 2nd ed. Cambridge, U.K.: Cambridge Univ. Press, 1992.
[13] J. W. Rockway and J. C. Logan, *Expert MININEC Broadcast Professional for Windows*. Carson City, NV: EM Scientific, 1999.
[14] L. K. Warne and K. C. Chen, "A simple transmission line model for narrow slot apertures having depth and losses," *IEEE Trans. Electromagn. Compat.*, vol. 34, no. 3, pp. 173–182, 1992.

Donald R. Wilton (S'63–M'65–SM'80–F'87) was born in Lawton, OK, on October 25, 1942. He received the B.S., M.S., and Ph.D. degrees from the University of Illinois at Urbana-Champaign, in 1964, 1966, and 1970, respectively.

From 1965 to 1968, he was with Hughes Aircraft Co., Fullerton, CA, engaged in the analysis and design of phased array antennas. From 1970 to 1983, he was with the Department of Electrical Engineering, University of Mississippi, and since 1983 he has been Professor of Electrical Engineering at the University of Houston, TX. From 1978 to 1979, he was a Visiting Professor at Syracuse University. During 2004 to 2005, he was a Visiting Scholar at the Polytechnic of Turin, Italy, the Sandia National Laboratories, and the University of Washington. His primary research interest is in computational electromagnetics, and he has published, lectured, and consulted extensively in this area.

Dr. Wilton is a member of Commission B of the International Union of Radio Science (URSI), in which he has held various offices including Chair of U. S. Commission B. He received the IEEE Third Millennium Medal. He has served the IEEE Antennas and Propagation Society as an Associate Editor of the TRANSACTIONS ON ANTENNAS AND PROPAGATION, as a Distinguished National Lecturer, and as a member of AdCom.

Nathan J. Champagne (S'87–M'97–SM'02) was born in New Orleans, LA, in 1966. He received the B.S., M.S., and Ph.D. degrees in electrical engineering from the University of Houston, Houston, TX, in 1988, 1991, and 1996, respectively.

From September 1994 to May 1995, he was an Intern at Matra Marconi Space in Toulouse, France. In November 1996, he joined Lawrence Livermore National Laboratory, Livermore, CA. He became an Assistant Professor of electrical engineering at Louisiana Tech University, Ruston, in May 2004. His research interests include engineering software design, computational electromagnetics on high performance computers, analyzing structures in a multilayered medium, thin-wire algorithms, and hybrid integral equation/finite element formulations.

Dr. Champagne is an associate member of Commission B of the International Union of Radio Science (URSI).